arXiv:1604.01966v1 [astro-ph.IM] 7 Apr 2016

ACTA ASTRONOMICA
Vol. **66** (2016) pp. 0–0

Analysis of photometric uncertainties in the OGLE-IV Galactic Bulge microlensing survey data[1]

J. Skowron[1], A. Udalski[1], S. Kozłowski[1], M.K. Szymański[1], P. Mróz[1], Ł. Wyrzykowski[1], R. Poleski[1,2], P. Pietrukowicz[1], K. Ulaczyk[1], M. Pawlak[1], and I. Soszyński[1]

[1] Warsaw University Observatory, Al. Ujazdowskie 4, 00-478 Warszawa, Poland
e-mail:jskowron@astrouw.edu.pl
[2] Department of Astronomy, Ohio State University, 140 West 18th Avenue, Columbus, OH 43210, USA

Received March 13, 2016

ABSTRACT

We present a statistical assessment of both, observed and reported, photometric uncertainties in the OGLE-IV Galactic bulge microlensing survey data. This dataset is widely used for the detection of variable stars, transient objects, discovery of microlensing events, and characterization of the exo-planetary systems. Large collections of RR Lyrae stars and Cepheids discovered by the OGLE project toward the Galactic bulge provide light curves based on this dataset. We describe the method of analysis, and provide the procedure, which can be used to update preliminary photometric uncertainties, provided with the light curves, to the ones reflecting the actual observed scatter at a given magnitude and for a given CCD detector of the OGLE-IV camera. This is of key importance for data modeling, in particular, for the correct estimation of the goodness of fit.

Key words: *surveys – techniques: photometric – methods: data analysis – instrumentation: detectors – stars: variables: general – gravitational lensing: micro*

1. Introduction

A fundamental part of any scientific inference is an assessment of the input data uncertainties. Any following results need to have the realm of validity specified. Also, any subsequent model parameters should have the uncertainties stated, but these in turn strongly depend on the level of trust we had in the input data.

The photometric studies of transient objects rely on our ability to firmly define the level of variability we trust is real. It is important to differentiate any true signal from the observational noise (*e.g.*, Udalski *et al.* 1994, Wyrzykowski *et al.* 2014,

[1] Based on observations obtained with the 1.3-m Warsaw telescope at the Las Campanas Observatory operated by the Carnegie Institution for Science.

Gould *et al.* 2015). On the other hand, most of the studies of periodic variable stars do not depend on the well-characterized uncertainties. These periodic signal can be found from the periodograms constructed only from the times and the flux measurements (*e.g.*, Pojmański 2002, Soszyński *et al.* 2014). However, for very detailed studies of periodic stars (asteroseismology) the robust knowledge of levels of the photometric uncertainties is important (*e.g.*, Smolec & Sniegowska 2016). Additionally, accurate modeling of eclipsing systems can benefit from good estimation of the photometric uncertainties (*e.g.*, Pilecki *et al.* 2013). This is true especially for those cases where the brightness of object varies significantly ($\gtrsim 1$ mag) since the relative weighting of the uncertainties varies between the magnitude ranges.

The OGLE project is a large-scale sky survey for variability. Its fourth phase (OGLE-IV, Udalski *et al.* 2015) is under way and is regularly monitoring 650 square degrees of the Magellanic System (mainly for variables, transients, supernovae, etc.), 130 square degrees of the Galactic bulge (microlensing, variables, novae) and 2200 square degrees of the Milky Way (variable stars, transient objects). The OGLE-IV survey uses the 1.3-m Warsaw telescope at the Las Campanas Observatory (of the Carnegie Institution for Science) equipped with the 32-CCD-chip mosaic camera with the field of view of 1.4 square degrees. Consult Udalski *et al.* (2015) for the detailed description of the project.

One of the key OGLE programs is monitoring of the Galactic bulge for the stellar variability with the cadence of 18 minutes to a couple of days. The observing season starts in February and lasts for nine months every year. Since 1994, the semi-automated system, *Early Warning System* (EWS), has been implemented to discover the on-going microlensing events candidates (Udalski *et al.* 1994).

The light curves of the discovered microlensing events candidates are presented on the web page `http://ogle.astrouw.edu.pl/ogle4/ews/ews.html` and are updated daily. These light curves are widely used by community in order to guide the follow-up efforts and to facilitate the real-time modeling and anomaly detection (Gould *et al.* 2015, Dominik *et al.* 2008, Bozza *et al.* 2012, to mention a few). Typically, the on-line data provide under-estimated instrumental uncertainties and it is a common practice to rescale them with the use of the best-fit microlensing model, in order to force the χ^2 per degree of freedom close to the unity (*e.g.*, Skowron *et al.* 2015).

The under-estimation of the uncertainties comes from two main sources. First, the Difference Image Analysis (DIA) pipeline calculates the expected uncertainty by propagation of the photon noise from the science frame onto the final measurement (Woźniak *et al.* 2000, Woźniak 2000). Since it is hard to reach the theoretical photon-noise levels with the real-world data, typical measurements have a slightly larger noise. Additionally, the reference image for the subtraction is regarded as noiseless. This is not strictly the case, especially if it is composed from the limited number of frames. Second, the assumed point spread function (PSF) might not fully model the observed shapes of the stellar profiles (Woźniak 2000). This has a

dominant effect at the bright end, where the uncertainties from the photon noise are far smaller than the uncertainties reported from the insufficient model of the PSF (*e.g.*, Fig. 3 of Woźniak 2000, and Fig. 2 of Wyrzykowski *et al.* 2009).

Due to the significant changes in magnitude, the analysis of microlensing events, detached eclipsing binaries, and cataclysmic variables is most susceptible to any problems with the uncertainties of individual measurements. There is no single factor which one can use in order to rescale the errorbars, and, that would be valid for the whole span of observed magnitudes. Hence, there is a need for a robust, empirical model of uncertainties and the procedure that would correct their values at any magnitude.

It this paper we analyze 5.4 years of data gathered since June 29, 2010 until November 8, 2015 (JD=2455377–2457335) in the 85 frequently visited fields of the microlensing survey toward the Galactic bulge (see Section 2). We present the analysis of the typical scatter observed in the photometric time series of all stars and compare it to the reported errorbars in the OGLE-IV light curves. We identify additional observational effects that have an impact on the observed scatter and which are not fully taken into account within the routinely reported error bars (Sections 3 and 4). We develop a series of functional forms to model the behavior of the true scatter across the whole magnitude range (Section 5). These forms depend on the particular detector, typical observing conditions at the site and the details of the photometric pipeline. We provide the procedure and all required coefficients to update photometric uncertainties of every measurement of the objects within this observational dataset (Section 6 and Appendix).

2. Data

Fig. 1 shows all fields that are monitored with the current microlensing survey, which is a part of OGLE-IV program since 2010. For the details of the observing strategy and location of all OGLE-IV fields toward the bulge see Udalski *et al.* (2015) or consult the web page `http://ogle.astrouw.edu.pl/sky/ogle4-BLG/`.

The photometric database of the OGLE-IV project contains observation times (HJD), magnitudes and uncertainties for all objects initially identified in the reference images. The observations are performed in the I-band and the V-band. The majority of measurements are performed with the former and between 300 and 13 000 epochs have already been collected for every microlensing field. These data are used for transients detection and searches for the periodic stars. The V-band observations have smaller cadence and between 10 and 120 have been acquired in each field with the goal to help characterize the discovered stars, microlensing events and to produce the Color Magnitude Diagrams (CMDs). Exposure times are 100 s and 150 s for the I- and V-band, respectively.

The OGLE-IV camera consists of 32 CCD detectors. Each has its own sensitivity, gain and read-out noise. The gains are fine-tuned in such a way, that the

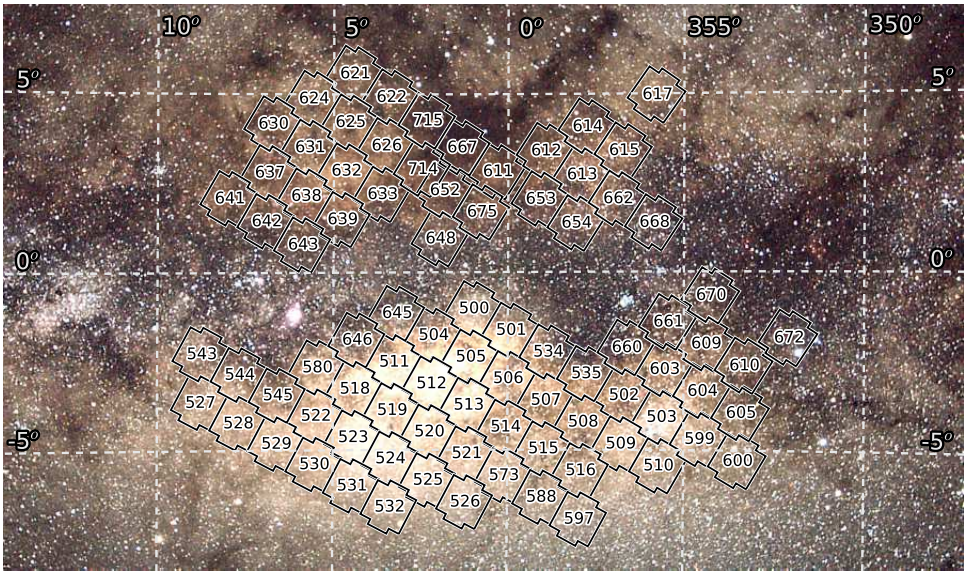

Fig. 1. Fields of the microlensing survey within the OGLE-IV project.

27.7 mag star would typically register 1 count within a 100 s exposure. Each observing field (*e.g.*, BLG672) are naturally divided into 32 subfields (chips) and referenced by adding a detector number (from 01 to 32) to the name of the field (*e.g.*, BLG672.08).

3. Model of the Pipeline-Reported Error Bars

All collected images are reduced with OGLE photometric pipeline based on the DIA photometry technique (Woźniak 2000). Each photometric data point has an uncertainty evaluated by the propagation of the photon noise estimated for each pixel of the image through the linear least-squares with the flat-fielding uncertainty added in the quadrature. The reference image is treated as noiseless.

Fig. 2 presents the the typical uncertainties reported for the I-band light curves. Each dot represents one object for which the mean weighted magnitude and the mean uncertainty of a random sample of 100 measurements was calculated. We show objects located in the field BLG500 and measured with the CCD detector no. 23 as an illustration. The exact values of the uncertainties, for a given brightness, vary by a few percent depending on the detector ($\approx 7\%$) and the field ($\approx 3\%$). All uncertainties equal to or below 3 mmag are treated as unrealistic. They are clipped to exactly 3 mmag in the photometric database and in the on-line light curves.

For each field and detector pair we characterize the typical uncertainties with a simple two-parameter model consisting of a Poisson noise contribution from the object and from the background. That is fitted to the empirical data – as presented in Fig. 2. The signal from the object of the mean brightness, m, is calculated with the Eq. 1, and the signal from the background is a parameter of the model (m_B).

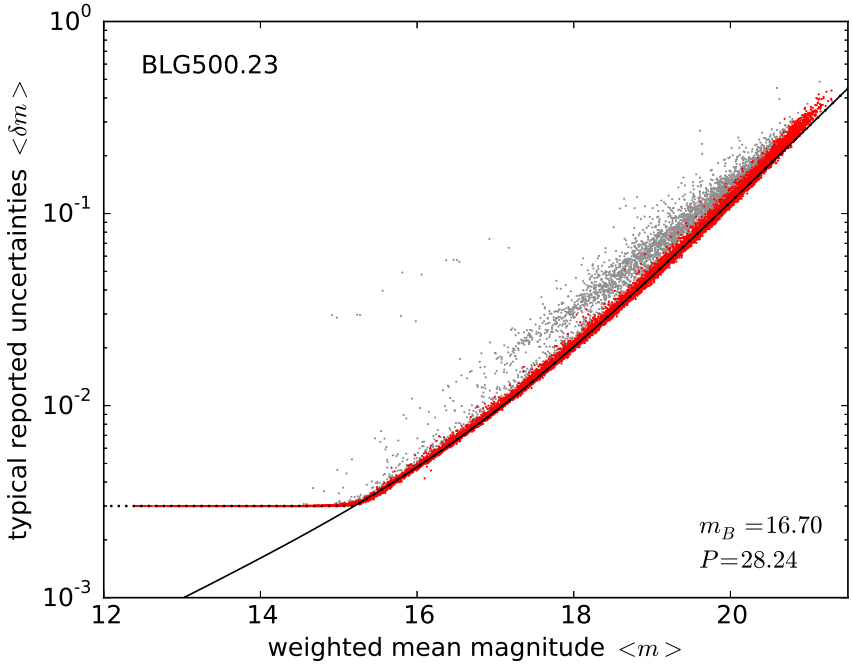

Fig. 2. Mean reported uncertainties *vs.* the mean magnitude of a star (red points) in the I-band. Each point represents the light curve of an individual star in the field. The data for the BLG500.23 field are shown for illustration. The exact behavior changes slightly depending on the field and on the CCD detector. The solid line shows the photon-noise model estimated by the fit to the typical uncertainties. The uncertainties with the values below 3 mmag, as not reliable, are clipped in the database to 3 mmag. The gray points represent the rejected, spurious objects – spikes near the bright stars and reflections at the edges of the camera.

The second parameter is a number that translates the brightness into the photon count (P) in the following way:

$$F = 10^{0.4(P-m)} \tag{1}$$

$$B = 10^{0.4(P-m_B)}. \tag{2}$$

Then, we estimate the noise as a square-root of the signal

$$\Delta F = \sqrt{F+B} \tag{3}$$

and translate it into the magnitude scale with

$$\Delta m = 2.5/\ln 10 \times \Delta F/F. \tag{4}$$

There are many more faint stars than the bright ones. In order for the fit to be more stable, we bin the sample in 50-100 bins in magnitude (depending on the number of stars in the given subfield) and calculate the median of the typical uncertainties within each bin. The input data consist of about a 100 pairs of magnitude

and uncertainty $(m_i, \delta m_i)$ to which the noise model is fitted with the least-squares method. We perform the fit in the magnitude range from ≈ 15.3 mag, where the errorbar values are meaningful, to 20.5 mag, above which the mean brightness measurement might be less reliable. The noise model fitted to the data ($\Delta m(m_i) = \delta m_i$) in the field BLG500.23 is shown with a solid line in Fig. 2. In the Appendix, we list the fitted values of P and m_B for each pair of the field and the detector in the data set.

4. Measurement of the Observational Scatter

In order to characterize the real observational uncertainty as a function of an object magnitude in a given field and given detector we analyze the light curves of all stars in this field. For each object we choose 100 random measurements from its time-series photometry and calculate the weighted mean magnitude and a root-mean-square scatter. Such data are presented in the Fig. 3 for a BLG543.15 field, where each dot represents a single object. The model of the typical uncertainties reported by the pipeline is presented as a black solid line. It is clear from the figure, that the uncertainties are under-estimated as the observed scatter for the majority of objects is larger than the noise model.

In the same fashion as in the previous Section, we divide the sample into 50-100 magnitude bins and find the value of scatter that is representative for every bin. We expect some of the stars to be variable, hence, we ignore 20% of points showing the largest scatter in the given bin and calculate the median of the remaining points. Then, we can fit for the scaling parameter (γ) which shifts the noise model to the value of the observed scatter (see Fig. 3).

For the stars brighter than $\sim$16th magnitude we see that there is an additional source of scatter that is not due to the photon noise. The scatter is consistent with the constant error level of a few millimagnitudes. This effect have already been found by various researchers – see Fig. 3 of Woźniak (2000) or Fig. 3 of Sumi *et al.* (2003). The constant error floor for the bright measurements is also routinely used in the process of rescaling error bars in the microlensing events analyzes (*e.g.*, Wyrzykowski *et al.* 2009, Skowron *et al.* 2016). Alard & Lupton (1998) and Woźniak (2000) suggest that the potential source of additional scatter is an inability of the mathematical PSF model to perfectly approximate the real-life seeing. The small deviations are not visible for the faint and moderate-brightness stars; this is noticeable only where the signal is strong and the photon noise small.

For each subfield we introduce the additional parameter, ε, aimed to model the level of the fixed error floor in the observed light curves. Then, for each measurement with the formal uncertainty, δm, that was performed with a given detector and in a given field, we can estimate the more optimal value of the uncertainty with $\sqrt{(\gamma\delta m)^2 + \varepsilon^2}$. The values of γ and ε for every subfield are tabulated in the Appendix. Fig. 3 presents this two-parameter model with respect to the observed

light-curve scatter.

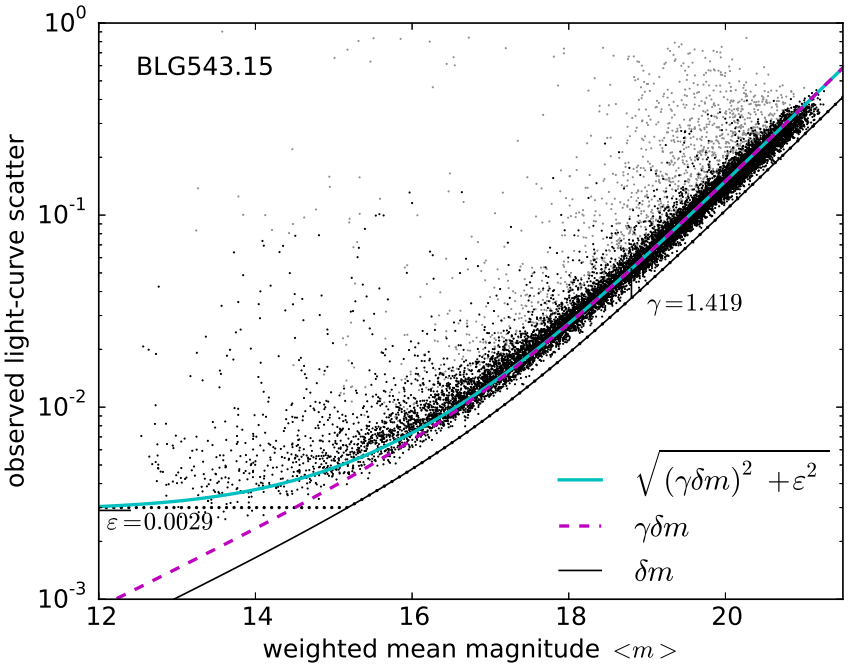

Fig. 3. Mean root mean square light-curve scatter as a function of the mean magnitude of a star (black points) in the I-band. Each point represents the light curve of an individual star in the field. The data for the BLG543.15 field are shown for illustration. The correction parameters slightly change, depending on the field and on the CCD detector. The black solid and dotted lines show the photon-noise model and typical reported uncertainties as in the Fig. 2. The magenta dashed line represents the noise model multiplied by a factor γ in order to match it to the observed scatter. The cyan solid line shows the same model, but with the additional constant error (ε) added in quadrature. This is the empirical term that dominates for the bright stars ($\sqrt{(\gamma\delta m)^2+\varepsilon^2}$). The gray points represent the rejected, spurious objects – spikes near the bright stars and reflections at the edges of the camera.

5. Model of the Observed Scatter

For the measurements fainter than ≈ 15.2 mag the values of errorbars provided in the light curves are typically greater than 3 mmag. These values carry some information about the conditions the image was taken under. The image parameters, like seeing and background have straight impact on the number of pixels that enters into the photon-noise estimation as well as the noise estimated within those pixels. For these measurements we employ the formula

$$\delta m_{i,\mathrm{new}} = \sqrt{(\gamma\delta m_i)^2+\varepsilon^2} \qquad (\mathrm{if}\ \delta m_i > 0.003), \tag{5}$$

where m_i is the original uncertainty. Note, that the P and m_B parameters introduced in Section 3 model only the median noise under typical seeing and background conditions at the survey site. In contrast, Eq. 5 is designed to conserve the information about the relative quality of each measurement.

All the uncertainties with values below 0.003 mag are not reliable, thus, we estimate the most likely uncertainty of such a measurement by taking into account only its brightness and comparing it to the typical scatter shown by the constant stars at the similar brightness. We use the model of the noise, as described in Sec. 3. We rescale it by γ and add the error floor ε in quadrature in order to better approximate the observational scatter for the bright stars. This averaged model for bright stars is presented with the green solid line in Fig. 4.

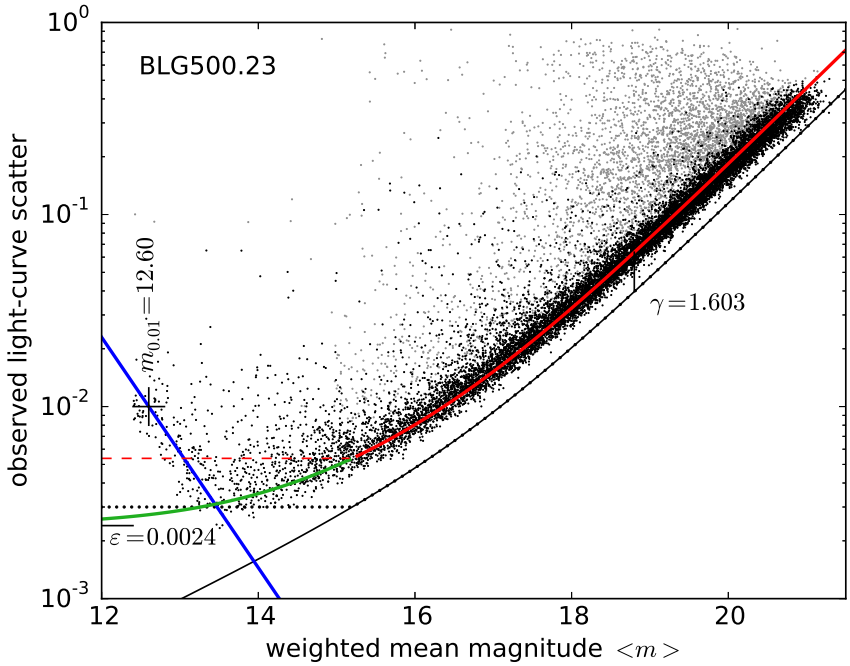

Fig. 4. Similar to Fig. 3 but with the final models of the scatter plotted. The blue, green and red solid lines represent three models of the light-curve scatter in the three, separate magnitude regimes: very bright (where non-linearity of the detector dominates), bright (where uncertainties are estimated from the photon-noise model), and remaining (where the majority of stars are and the canonical scaling of the uncertainties by $\sqrt{(\gamma\delta m)^2+\varepsilon^2}$ is possible).

We note, that there is, however, a yet another source of scatter that is evident for the very brightest stars ($I \lesssim 13$ mag). There is a very fast rising trend of scatter with the increasing brightness. This was not present in the OGLE-II data (see Fig. 2 of Wyrzykowski *et al.* 2009) nor in the OGLE-III data (*cf.* Wyrzykowski *et al.* 2011). In the laboratory studies, the CCD detectors of the OGLE-IV camera do show slight level of non-linear response ($\approx 0.1-0.3\%$) for pixels with 100k

electrons. This corresponds to about 52k–62k counts depending on the gain of a particular detector. The limit above which the pixel is not measured by the pipeline is 65 535 counts. This might be an explanation for a very fast raise of uncertainties for extremely bright objects where the central pixels are close to this limit.

The fast rise of uncertainties is consistent with the scatter of flux being proportional to $\sim F^{5/2}$ (where F is the observed flux). This is an empirical approximation, however, it is in an good agreement with the data from the various fields and detectors. We parametrize this effect by providing the magnitude value, $m_{0.01}$, at which the expected scatter for constant stars is equal to 0.01 mag. Since the slope is fixed, we can provide a one-parameter formula for the uncertainty due to this effect for every photometric measurement m_i in the form:

$$\Delta m_{nonlinear,i} = 0.01 \times 10^{0.6(m_{0.01}-m_i)} \tag{6}$$

During the estimation of the single-parameter $m_{0.01}$ we notice that it has very similar value for the same CCD detector across multiple observing fields. This further strengthens the argument, that it is a feature of the particular detector. Since the number of very bright stars is limited, we can merge data from various fields in order to robustly estimate the value of $m_{0.01}$ for any of 32 detectors. In order not to overestimate the typical scatter for the very bright stars, instead of a median, we choose $m_{0.01}$ in such a way that only 15 percent of points lie below the model described by Eq. 6. This is done, because the distribution of scatter values form the brightest stars is not Gaussian, and 15th percentile lies closer to the mode of the distribution than the mean or the median.

With the better understanding of the non-linear behavior of CCD detectors and with additional information about conditions of a particular exposure (seeing, background) it is possible to better estimate magnitude and uncertainty of a measurement. Here, we only provide a statistical formula that describes the typical expected scatter from this effect and can be used with an absence of any additional information.

6. Correction Procedure for the Uncertainties

Any light curve from the OGLE-IV real-time data analysis systems (Udalski 2008, Udalski *et al.* 2015, Mróz *et al.* 2015b), the on-going microlensing event from the Early Warning System[2] or the light curve from the early catalogs of variable stars based on the OGLE-IV Galactic bulge data (*e.g.*, Poleski *et al.* 2011, Mróz *et al.* 2015a), can be corrected using the procedure described in this Section. The uncertainties rescaled based on the statistical behavior of the neighboring constant stars can facilitate the detailed modeling of the individual objects.

The full procedure is described in the next paragraph. The input to the procedure consist of two values: the magnitude and the uncertainty of the individual

[2] `http://ogle.astrouw.edu.pl/ogle4/ews/ews.html`

measurement $(m_i, \delta m_i)$ from the OGLE-IV light curve. One has to also know the observed field and the particular detector the measurement was taken with. The Appendix lists the five parameters for every field and CCD chip pair. These parameters are as follows: the scale of the level of errorbar underestimation (γ), the constant error floor, which dominates for the bright measurements (ε), the approximated counts-to-magnitudes conversion unit (P), the value parameterizing the background noise (m_B), and the magnitude at which the scatter from the non-linearity effect of the detector reaches 0.01 magnitudes ($m_{0.01}$). The detailed meaning of each parameters are described in previous Sections.

The procedure is as follows:

Input: $(m_i, \delta m_i)$ – a photometric data point of interest and $(\gamma, \varepsilon, P, m_B, m_{0.01})$ – the coefficients for the given FIELD.CHIP pair

if $\delta m_i > 0.003$ mag **then**

$\delta m_{\mathrm{new},i} = \sqrt{(\gamma \delta m_i)^2 + \varepsilon^2}$

else

$\Delta m_{nonlinear} = 0.01 \times 10^{0.6(m_{0.01} - m_i)}$ – model of non-linearity ($\sim F^{5/2}$)

$F = 10^{0.4(P - m_i)}$ – approximate number of photons from the star

$B = 10^{0.4(P - m_B)}$ – approximate number of background photons contributing to the noise

$\Delta F = \sqrt{F + B}$ – photon noise model

$\Delta m_{bright} = 2.5 / \ln 10 \times \Delta F / F$ – estimated noise in magnitudes

$\delta m_{\mathrm{new},i} = max\left[\delta m_i, \sqrt{(\gamma \Delta m_{bright})^2 + \varepsilon^2}, \Delta m_{nonlinear}\right]$

end if

Output: $(m_i, \delta m_{\mathrm{new},i})$

The output from the procedure is the new value of the uncertainty, which goal is to provide the better estimation of the expected accuracy of the measurement.

7. Conclusions

We have performed statistical analysis of the typical light-curve scatter in the OGLE-IV Galactic bulge microlensing survey data. The scatter for non-variable stars was compared to the mean uncertainty reported by the photometric pipeline at various magnitudes. The amount of errorbar underestimation was measured for every field and every detector and it is typically between 10% and 70%. The scaling values (γ) are presented in the Appendix.

We found additional effects that should be taken into account within the light-curve errorbars. Most importantly, the existence of a constant error floor, which affects the uncertainties of brighter measurements ($\lesssim 15$ mag) and is parametrized by ε (typically ≈ 2.8 mmag).

The scatter of 12–13 mag stars is much greater than the scatter of 13–14 mag stars. This is a likely effect of the non-linearity of the CCD detectors for the very large signals. We find that the rise of the scatter with the increasing flux of the star

can be described by the power law ($\sim F^{5/2}$) and we measure this effect for every CCD detector of the OGLE-IV camera.

The detailed procedure for correcting the values of reported uncertainties is provided in Section 6. This procedure can be applied to any light curve in the discussed fields in order to facilitate the analysis of variable stars and transient objects.

Finally, in the Appendix, we provide the values needed as an inputs to the above mentioned procedure. These values are quoted for every subfield of the survey and were estimated from the analysis of light curves of all objects within the given region.

Acknowledgements. We would like to thank Profs. M. Kubiak and G. Pietrzyński, former members of the OGLE team, for their contribution to the collection of the OGLE photometric data over the past years. The OGLE project has received funding from the National Science Center, Poland, grant MAESTRO 2014/14/A/ST9/00121 to Andrzej Udalski.

REFERENCES

Alard, C., & Lupton, R. H. 1998, *ApJ*, **503**, 325.
Bozza, V., Dominik, M., Rattenbury, N. J., *et al.* 2012, *MNRAS*, **424**, 902.
Dominik, M., Horne, K., Allan, A., *et al.* 2008, *Astronomische Nachrichten*, **329**, 248.
Gould, A., Yee, J., & Carey, S. 2015, *Spitzer Proposal*, **12013**, .
Mróz, P., Udalski, A., Poleski, R., *et al.* 2015a, *ApJS*, **219**, 26.
Mróz, P., Udalski, A., Poleski, R., *et al.* 2015b, *Acta Astron.*, **65**, 313.
Pilecki, B., Graczyk, D., Pietrzyński, G., *et al.* 2013, *MNRAS*, **436**, 953.
Pojmański, G. 2002, *Acta Astron.*, **52**, 397.
Poleski, R., Udalski, A., Skowron, J., *et al.* 2011, *Acta Astron.*, **61**, 123.
Skowron, J., Shin, I.-G., Udalski, A., *et al.* 2015, *ApJ*, **804**, 33.
Skowron, J., Udalski, A., Poleski, R., *et al.* 2016, *ApJ*, **820**, 4.
Smolec, R., & Sniegowska, M. 2016, *MNRAS*, **458**, 3561.
Soszyński, I., Udalski, A., Szymański, M. K., *et al.* 2014, *Acta Astron.*, **64**, 177.
Sumi, T., Abe, F., Bond, I. A., *et al.* 2003, *ApJ*, **591**, 204.
Udalski, A., Szymański, M., Kałużny, J., *et al.* 1994, *Acta Astron.*, **44**, 227.
Udalski, A. 2008, *Acta Astron.*, **58**, 187.
Udalski, A., Szymański, M. K., & Szymański, G. 2015, *Acta Astron.*, **65**, 1.
Woźniak, P. R., Alard, C., Udalski, A., *et al.* 2000, *ApJ*, **529**, 88.
Woźniak, P. R. 2000, *Acta Astron.*, **50**, 421.
Wyrzykowski, Ł., Kozłowski, S., Skowron, J., *et al.* 2009, *MNRAS*, **397**, 1228.
Wyrzykowski, L., Skowron, J., Kozłowski, S., *et al.* 2011, *MNRAS*, **416**, 2949.
Wyrzykowski, Ł., Kostrzewa-Rutkowska, Z., Kozłowski, S., *et al.* 2014, *Acta Astron.*, **64**, 197.

A Error-bar correction coefficients for every FIELD.CHIP pair

Below we present the coefficients for the uncertainty-correction procedure described in Sec. 6. The full on-line tables are available at WWW address:

`http://ogle.astrouw.edu.pl/ogle4/errorbars/blg/`
and FTP address:
`ftp://ftp.astrouw.edu.pl/ogle/ogle4/errorbars/`.

CCD	γ	ε	P	m_B	$m_{0.01}$	CCD	γ	ε	P	m_B	$m_{0.01}$
BLG501 (*I*-band)											
.01	1.731	0.0030	28.215	16.217	12.491	.02	1.651	0.0030	28.233	16.317	12.354
.03	1.663	0.0032	28.252	16.344	12.734	.04	1.696	0.0031	28.258	16.367	12.453
.05	1.724	0.0028	28.268	16.437	12.495	.06	1.664	0.0028	28.262	16.547	12.524
.07	1.686	0.0028	28.278	16.671	12.641	.08	1.756	0.0031	28.231	16.055	12.659
.09	1.650	0.0028	28.241	16.234	12.557	.10	1.660	0.0030	28.254	16.246	12.581
.11	1.677	0.0031	28.265	16.325	12.374	.12	1.769	0.0034	28.277	16.379	12.655
.13	1.671	0.0031	28.278	16.457	12.323	.14	1.687	0.0025	28.296	16.526	12.367
.15	1.627	0.0024	28.299	16.713	12.258	.16	1.754	0.0030	28.266	16.617	12.530
.17	1.804	0.0029	28.228	16.080	12.488	.18	1.689	0.0031	28.230	16.218	12.800
.19	1.738	0.0030	28.246	16.222	12.573	.20	1.722	0.0029	28.258	16.247	12.567
.21	1.784	0.0037	28.280	16.316	12.487	.22	1.677	0.0029	28.289	16.442	12.421
.23	1.669	0.0028	28.288	16.535	12.602	.24	1.706	0.0024	28.315	16.634	12.300
.25	1.653	0.0027	28.284	16.698	12.400	.26	1.754	0.0028	28.247	16.275	12.370
.27	1.735	0.0027	28.256	16.391	12.334	.28	1.706	0.0030	28.268	16.462	12.772
.29	1.713	0.0031	28.273	16.459	12.660	.30	1.609	0.0029	28.287	16.687	12.361
.31	1.615	0.0025	28.289	16.691	12.370	.32	1.474	0.0027	28.300	17.038	12.474
BLG505 (*I*-band)											
.01	1.575	0.0033	28.096	16.281	12.491	.02	1.480	0.0029	28.099	16.353	12.354
.03	1.527	0.0033	28.111	16.315	12.734	.04	1.519	0.0030	28.106	16.342	12.453
.05	1.541	0.0030	28.109	16.400	12.495	.06	1.526	0.0029	28.116	16.374	12.524
.07	1.532	0.0032	28.104	16.348	12.641	.08	1.564	0.0039	28.095	16.266	12.659
.09	1.456	0.0032	28.101	16.425	12.557	.10	1.489	0.0029	28.108	16.347	12.581
.11	1.486	0.0030	28.124	16.372	12.374	.12	1.547	0.0037	28.122	16.398	12.655
.13	1.495	0.0030	28.122	16.381	12.323	.14	1.500	0.0029	28.127	16.386	12.367
.15	1.466	0.0026	28.127	16.395	12.258	.16	1.628	0.0032	28.113	16.186	12.530
.17	1.653	0.0030	28.098	16.194	12.488	.18	1.563	0.0034	28.105	16.273	12.800
.19	1.579	0.0026	28.104	16.223	12.573	.20	1.572	0.0029	28.117	16.266	12.567
.21	1.581	0.0033	28.118	16.297	12.487	.22	1.486	0.0031	28.116	16.460	12.421
.23	1.486	0.0030	28.114	16.452	12.602	.24	1.514	0.0029	28.139	16.371	12.300
.25	1.550	0.0032	28.109	16.289	12.400	.26	1.611	0.0027	28.118	16.306	12.370
.27	1.569	0.0026	28.110	16.359	12.334	.28	1.559	0.0032	28.112	16.373	12.772
.29	1.549	0.0030	28.106	16.334	12.660	.30	1.423	0.0031	28.117	16.512	12.361
.31	1.448	0.0028	28.117	16.433	12.370	.32	1.345	0.0037	28.140	16.694	12.474
BLG512 (*I*-band)											
.01	1.731	0.0026	28.256	16.273	12.491	.02	1.639	0.0024	28.264	16.356	12.354
.03	1.661	0.0025	28.274	16.322	12.734	.04	1.702	0.0025	28.267	16.292	12.453
.05	1.744	0.0023	28.275	16.321	12.495	.06	1.688	0.0023	28.268	16.371	12.524
.07	1.708	0.0027	28.266	16.343	12.641	.08	1.703	0.0028	28.242	16.238	12.659
.09	1.620	0.0025	28.260	16.365	12.557	.10	1.636	0.0025	28.267	16.329	12.581
.11	1.651	0.0024	28.267	16.318	12.374	.12	1.760	0.0028	28.269	16.259	12.655
.13	1.674	0.0024	28.269	16.299	12.323	.14	1.683	0.0024	28.274	16.280	12.367
.15	1.649	0.0022	28.273	16.283	12.258	.16	1.835	0.0026	28.268	16.042	12.530
.17	1.783	0.0027	28.241	16.283	12.488	.18	1.660	0.0025	28.259	16.369	12.800
.19	1.730	0.0022	28.254	16.308	12.573	.20	1.707	0.0024	28.259	16.262	12.567
.21	1.747	0.0027	28.257	16.230	12.487	.22	1.668	0.0024	28.261	16.263	12.421
.23	1.660	0.0023	28.271	16.278	12.602	.24	1.672	0.0024	28.276	16.282	12.300

.25	1.708	0.0027	28.265	16.180	12.400	.26	1.750	0.0021	28.251	16.347	12.370
.27	1.726	0.0020	28.262	16.410	12.334	.28	1.683	0.0025	28.256	16.388	12.772
.29	1.716	0.0023	28.254	16.277	12.660	.30	1.599	0.0024	28.254	16.389	12.361
.31	1.600	0.0025	28.267	16.397	12.370	.32	1.486	0.0031	28.275	16.627	12.474

. . . table abbreviated, see on-line material.

Table 1: The errorbar-correction coefficients for the *I*-band data from the 1.3-m Warsaw Telescope made with the 32-CCD-chip mosaic OGLE-IV camera. The observing fields in the table are from the on-going microlensing survey toward the Galactic bulge. The full contents of this table is available on-line at *ftp://ftp.astrouw.edu.pl/ogle/ogle4/errorbars/errcorr-OIV-BLG-I.dat*.

CCD	γ	ε	P	m_B	$m_{0.01}$	CCD	γ	ε	P	m_B	$m_{0.01}$
BLG500 (*V*-band)											
.01	1.468	0.0032	28.838	18.097	13.286	.02	1.392	0.0026	28.852	18.398	13.108
.03	1.435	0.0027	28.880	18.459	13.515	.04	1.453	0.0026	28.876	18.540	13.186
.05	1.538	0.0027	28.872	18.652	13.186	.06	1.487	0.0023	28.881	18.685	13.241
.07	1.580	0.0028	28.899	18.634	13.363	.08	1.410	0.0028	28.847	18.207	13.481
.09	1.393	0.0024	28.864	18.354	13.330	.10	1.407	0.0025	28.870	18.458	13.310
.11	1.441	0.0027	28.880	18.558	13.068	.12	1.483	0.0032	28.872	18.536	13.383
.13	1.439	0.0027	28.881	18.598	13.003	.14	1.469	0.0020	28.890	18.612	13.041
.15	1.436	0.0023	28.893	18.660	12.919	.16	1.588	0.0034	28.884	18.485	13.213
.17	1.473	0.0031	28.855	18.426	13.202	.18	1.460	0.0026	28.868	18.471	13.570
.19	1.512	0.0025	28.882	18.484	13.299	.20	1.464	0.0026	28.884	18.447	13.255
.21	1.481	0.0030	28.871	18.491	13.184	.22	1.432	0.0023	28.888	18.511	13.073
.23	1.470	0.0026	28.886	18.594	13.312	.24	1.471	0.0029	28.877	18.657	13.017
.25	1.424	0.0034	28.868	18.609	13.019	.26	1.603	0.0025	28.885	18.595	12.996
.27	1.611	0.0025	28.884	18.660	12.977	.28	1.483	0.0036	28.879	18.660	13.536
.29	1.555	0.0027	28.879	18.580	13.348	.30	1.388	0.0026	28.874	18.758	13.037
.31	1.410	0.0029	28.881	18.683	13.030	.32	1.313	0.0035	28.870	18.972	12.846
BLG501 (*V*-band)											
.01	1.482	0.0028	28.828	18.175	13.286	.02	1.406	0.0024	28.832	18.327	13.108
.03	1.422	0.0027	28.856	18.343	13.515	.04	1.442	0.0025	28.866	18.406	13.186
.05	1.516	0.0023	28.875	18.467	13.186	.06	1.491	0.0025	28.872	18.560	13.241
.07	1.580	0.0035	28.876	18.620	13.363	.08	1.455	0.0030	28.839	17.965	13.481
.09	1.419	0.0024	28.851	18.178	13.330	.10	1.410	0.0025	28.860	18.238	13.310
.11	1.431	0.0024	28.869	18.358	13.068	.12	1.508	0.0032	28.870	18.492	13.383
.13	1.438	0.0025	28.881	18.538	13.003	.14	1.493	0.0024	28.889	18.570	13.041
.15	1.437	0.0025	28.888	18.698	12.919	.16	1.590	0.0040	28.880	18.476	13.213
.17	1.460	0.0026	28.826	18.014	13.202	.18	1.460	0.0024	28.837	18.150	13.570
.19	1.497	0.0024	28.853	18.244	13.299	.20	1.471	0.0025	28.867	18.275	13.255
.21	1.490	0.0029	28.878	18.419	13.184	.22	1.451	0.0026	28.886	18.496	13.073
.23	1.468	0.0028	28.885	18.585	13.312	.24	1.499	0.0027	28.899	18.618	13.017
.25	1.431	0.0029	28.884	18.547	13.019	.26	1.538	0.0022	28.862	18.224	12.996
.27	1.572	0.0016	28.870	18.415	12.977	.28	1.470	0.0026	28.872	18.531	13.536
.29	1.540	0.0029	28.880	18.506	13.348	.30	1.410	0.0032	28.873	18.702	13.037
.31	1.411	0.0027	28.885	18.598	13.030	.32	1.314	0.0032	28.885	18.892	12.846
BLG502 (*V*-band)											
.01	1.356	0.0041	28.791	18.362	13.286	.02	1.299	0.0038	28.797	18.549	13.108
.03	1.311	0.0034	28.805	18.495	13.515	.04	1.307	0.0031	28.809	18.440	13.186
.05	1.399	0.0032	28.818	18.480	13.186	.06	1.343	0.0027	28.810	18.511	13.241
.07	1.395	0.0030	28.810	18.489	13.363	.08	1.288	0.0048	28.782	18.315	13.481

.09	1.278	0.0038	28.790	18.537	13.330	.10	1.295	0.0035	28.800	18.588	13.310
.11	1.326	0.0032	28.805	18.624	13.068	.12	1.419	0.0043	28.794	18.665	13.383
.13	1.351	0.0037	28.808	18.600	13.003	.14	1.363	0.0023	28.813	18.507	13.041
.15	1.297	0.0023	28.811	18.533	12.919	.16	1.387	0.0030	28.794	18.313	13.213
.17	1.331	0.0044	28.773	18.416	13.202	.18	1.332	0.0035	28.794	18.484	13.570
.19	1.399	0.0033	28.795	18.489	13.299	.20	1.360	0.0030	28.806	18.420	13.255
.21	1.333	0.0034	28.798	18.465	13.184	.22	1.307	0.0025	28.803	18.484	13.073
.23	1.314	0.0031	28.808	18.520	13.312	.24	1.351	0.0028	28.808	18.515	13.017
.25	1.282	0.0027	28.783	18.393	13.019	.26	1.433	0.0032	28.799	18.471	12.996
.27	1.463	0.0026	28.807	18.577	12.977	.28	1.343	0.0033	28.801	18.570	13.536
.29	1.370	0.0039	28.798	18.499	13.348	.30	1.261	0.0026	28.789	18.632	13.037
.31	1.273	0.0026	28.794	18.566	13.030	.32	1.206	0.0031	28.786	18.877	12.846

. . . table abbreviated, see on-line material.

Table 2: The errorbar-correction coefficients for the *V*-band data from the 1.3-m Warsaw Telescope made with the 32-CCD-chip mosaic OGLE-IV camera. The observing fields in the table are from the on-going microlensing survey toward the Galactic bulge. The full contents of this table is available on-line at *ftp://ftp.astrouw.edu.pl/ogle/ogle4/errorbars/errcorr-OIV-BLG-V.dat*.